Research paper

A spent upper stage removal mission aimed to reduce debris impact footprint size

Vladimir S. Aslanov[*], Dmitry A. Sizov

Samara National Research University, 34, Moscovskoe shosse, Samara 443086, Russia

ABSTRACT

A process of a spent upper stage removal from low Earth orbit is considered, which consists of three phases: towing of the stage using a tether; descent of the stage into the low-density atmosphere; motion of its debris fragments after the breakup caused by the aerodynamic and thermal loads. It is shown that the attitude motion of the stage during its descent largely affects its breakup altitude and consequently the size of debris impact footprint and its position on the surface of the Earth. A certain number of ways to reduce the footprint extent are proposed. As an example of using the proposed method, a numerical simulation of the removal of a spent Ariane 4 upper stage H10 was performed. The results of the study can be used for planning missions to clean up space debris from low Earth orbit.

1. Introduction

The number of non-functioning objects in orbit around the Earth is increasing every year. Therefore, the probability of their collisions with each other is also growing. A single collision may increase the total number of space debris by several thousand. In this regard, the international community is making significant efforts to develop the active debris removal (ADR) systems [1]. One of the important classes of potential targets for future ADR are the spent rocket stages (rocket bodies). Their total mass is about 3000 tons, and a third of this mass is in low earth orbit (LEO) [2]. The active de-orbiting of a massive object from LEO can be performed using a chaser, which can be either a specially designed spacecraft [3] or a modified upper stage of a launch vehicle [4]. A specially designed spacecraft can carry a significant amount of fuel, so it is possible to de-orbit a couple dozen objects in one mission [5,6]. In the case of using an upper stage of a launch vehicle, it is assumed that, after completion of the main mission, it de-orbits a certain number of objects, capturing them with a harpoon [7] or net [8] and using a tether for transportation. The number of de-orbited objects in this case depends on the amount of residual fuel in the tug, but one may expect that it will be substantially lower than in the first case. However, the advantage of the upper stages of launch vehicles is the ability to produce significant thrust [4].

The mission aimed at de-orbiting several objects can be carried out under two scenarios [9]. The first scenario involves attaching a deorbiting kit to the object. The deorbiting kit can be either a small engine

[3] or electrodynamic tether creating a Lorenz force [5]. Following the second scenario, which is discussed in this paper, the chaser approaches the selected target, reduces its periapsis altitude to a value that ensures the object's independent re-entry into the atmosphere, then goes to another target and eventually re-enters the atmosphere. To reduce the periapsis altitude of the target, the chaser must apply a force to it. This force may have different nature. One way is to create a tension force using a tether. The second way is the contactless removal using Coulomb electrostatic force [10] or an ion beam [11].

In any case, the final phase of removal of any object is its disintegration into fragments in the atmosphere. These fragments can pose a threat to both aircraft and ground objects. Therefore, of great importance is the size of the debris impact footprint, which mainly depends on the altitude at which the breakup occurs. The breakup altitude is influenced not only by the motion of the center of mass of the object, but also by its attitude motion. The latter, in turn, depends both on the aerodynamic characteristics of the object and on the initial conditions of its descent (velocity, flight path angle, altitude) after separation from the chaser. These initial conditions are determined by the amount of change in object velocity caused by the interaction with the chaser. There are several analysis tools for simulating the breakup of objects of various shapes due to structural and thermal loads during the descent into the atmosphere, a detailed review of which is given in Ref. [12]. These tools, in our opinion, provide unique opportunities to validate already proposed ADR missions. But in order to synthesize new solutions, more research is needed. The goal of this paper is to create a

[*] Corresponding author.
E-mail addresses: aslanov_vs@mail.ru (V.S. Aslanov), sizov.syzran@gmail.com (D.A. Sizov).
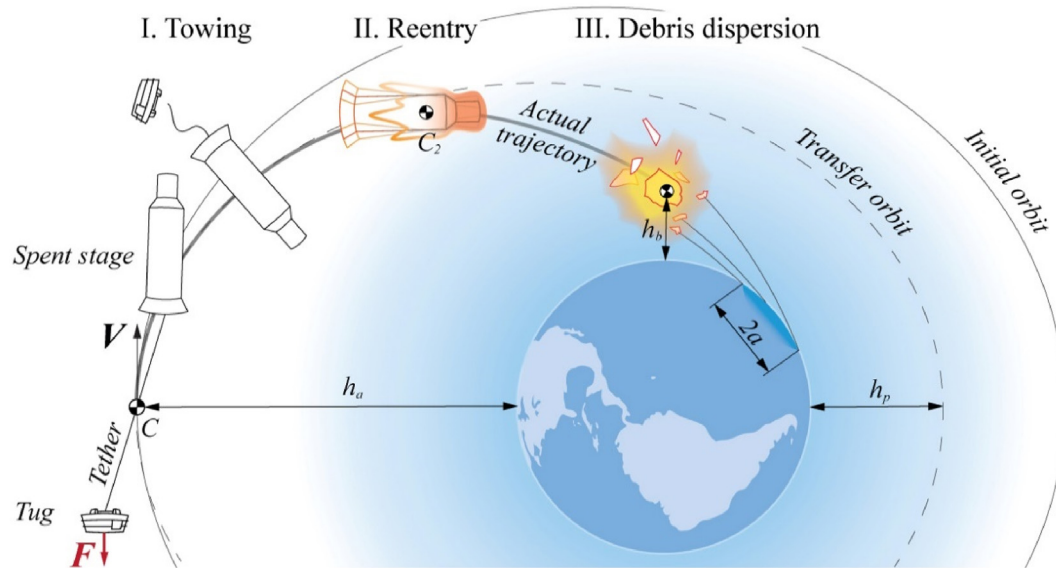
Fig. 1. Phases of the removal process.

method for estimating the size of the debris impact footprint on the surface of the Earth, taking into account the attitude motion of the object. This method will allow to reduce the footprint size by determination of the key mission parameters, e.g., the amount of force applied by the chaser, the perigee altitude of the stage after the separation, the initial conditions of its attitude motion.

The paper consists of three main sections. In Section 2 the problem is formulated. The ADR process is divided into three phases. In Section 3 the equations of motion for each phase are formulated. In Section 4 a numerical example is considered. The influence of the parameters of the system on the size of the debris impact footprint is examined.

2. Problem statement

Consider the problem of deorbiting a spent upper stage using a tug. During the process, the number of bodies in the system, their mass and shape change. Therefore, it is advisable to divide this process into three phases (Fig. 1).

In the first phase, the towing near the stage apogee at the altitude h_a is performed. The goal is to lower the periapsis of the stage to a value h_p that provides its reentry into the atmosphere within a few months. Analysis of the first phase allows to obtain the required thrust, the duration of towing, and the altitude of separation. The latter should be as high as possible, since this will allow the tug to save fuel and deorbit other objects.

The second phase begins after the separation of the tug. During this phase, the stage descends into the low-density atmosphere. As a rule, the center of mass of rocket bodies is significantly shifted relative to the center of pressure. This causes the aerodynamic stabilization of their rotation relative to the center of mass even in the presence of residual angular velocity after separation from the tug. The aerodynamic loads will be lower if the altitude at which the oscillation begins will be higher. Therefore, in order to reduce the size of the debris impact footprint on the surface of the Earth, it is advisable to ensure that the altitude of the aerodynamic stabilization is as high as possible. When the loads exceed a certain limit, the breakup of the stage occurs. The case of planar motion is the most unfavorable, since the same areas of the stage are cyclically affected by aerodynamic and thermal loads, which leads to uneven heating and can also cause fatigue cracking. Analysis of the second phase allows to estimate the breakup altitude h_b taking into account the aerodynamic characteristics of the stage and its attitude motion.

The third phase begins immediately after the breakup. From this moment on, one has to study the motion of individual debris fragments, each of them having its own set of parameters. Since the breakup of the stage can be accompanied by an explosion, not only the aerodynamic characteristics of the fragments can vary, but also the magnitude and direction of their initial velocities. Finally, the analysis of the fragments trajectories allows to estimate the extent of the debris impact footprint.

3. Mathematical models

3.1. General remarks

This section provides mathematical models, which, in the authors' opinion, are the most convenient for describing the motion of the system at each of the above phases of the ADR process. The initial conditions for each subsequent phase are obtained from the previous one.

At the towing phase, the orbital elements are used to define the motion of the center of mass of the system. In this case, it is easy to describe the acceleration of the center of mass due to the tug thrust, since it is directed along the local horizontal. Osculating elements also give a simple way to express the center of mass perigee altitude. Towing ends when the required perigee altitude is reached. At the reentry phase, the motion of the center of mass of the stage is described using the geodetic and flight path coordinate frames, which are traditional for reentry analysis. This allows to obtain velocity, altitude and flight path angle of the center of mass. We examine as well the attitude motion of the stage, determined by the angle of attack, until the shape of the stage changes due to its disintegration into separate debris fragments. At the third phase, we study the motion of the fragments with different ballistic coefficients. The motion of an individual fragment is described by almost the same equations as the motion of the center of mass of the stage at the previous phase.

We impose the following assumptions:

1. The Earth is spherical and not rotating.
2. Air density changes with altitude according to the US Standard Atmosphere 1976 [13].
3. In the towing phase, the influence of the atmosphere is negligible and the mass of the system is constant.
4. The velocity of the center of mass of the stage after towing is equal to the velocity of the center of mass of the system.

5. The motion of the stage during the descent is planar.
6. The aerodynamic characteristics of the stage do not depend on the Mach number.
7. In the dispersion phase, since the form of the debris fragments is unpredictable, the absence of lift force is assumed.

3.2. Towing

In this phase, the motion of the center of mass of the system is considered (Fig. 1). If the tug thrust F is directed along the local horizontal, the Gauss planetary equations [14] can be written as follows:

$$\frac{dh}{dt} = r a_\theta, \tag{1}$$

$$\frac{de}{dt} = \frac{(h^2 + \mu r)\cos\theta + \mu e r}{\mu h} a_\theta, \tag{2}$$

$$\frac{d\omega}{dt} = \frac{\left(\frac{h^2}{\mu} + r\right)\sin\theta}{eh} a_\theta, \tag{3}$$

$$\frac{d\theta}{dt} = \frac{h}{r^2} - \frac{\left(\frac{h^2}{\mu} + r\right)\sin\theta}{eh} a_\theta, \tag{4}$$

where h is the specific angular momentum, e is the orbit eccentricity, ω the argument of periapsis, θ is the true anomaly, $r = \frac{h^2}{\mu(1 + e\cos\theta)}$ is the distance from the center of the Earth, $a_\theta = -\frac{F}{m_1 + m_2}$ is the acceleration caused by the tug thrust, μ is the gravitational parameter of the Earth, m_1 the mass of the tug, m_2 is the mass of the stage.

3.3. Reentry

The motion of the center of mass of the stage and its rotation relative to this point during the descent in the low-density atmosphere (Fig. 1) are described by the following equations [15]:

$$\dot{V} = -\frac{D}{m_2} - g\sin\gamma, \tag{5}$$

$$\dot{\gamma} = \frac{L}{m_2} - \frac{g\cos\gamma}{V} + \frac{V\cos\gamma}{r}, \tag{6}$$

$$\dot{r} = V\sin\gamma, \tag{7}$$

$$\dot{\theta} = \frac{V\cos\gamma}{r}, \tag{8}$$

$$\ddot{\alpha} = \frac{M_z(\alpha, \dot{\alpha})}{J_z} + J_z(\ddot{\gamma} - \ddot{\theta}), \tag{9}$$

where V is the velocity, $g = \frac{\mu}{r^2}$ is the gravitational acceleration, α is the angle of attack (Fig. 2), γ is the flight path angle, $D = C_D(\alpha)Aq$ is the aerodynamic drag of the stage, $L = C_L(\alpha)Aq$ is the aerodynamic lift, $M_z(\alpha, \dot{\alpha})$ is the aerodynamic torque, J_z is the principal moment of inertia of the stage about an axis normal to the orbit plane, A is the reference area, C_D and C_L are the drag and lift coefficients, respectively, $q = \frac{\rho V^2}{2}$ is the dynamic pressure, ρ is the air density. The aerodynamic torque can be written as follows:

$$M_z(\alpha, \dot{\alpha}) = \left(C_m(\alpha) + C_m^{\dot{\alpha}}\frac{\dot{\alpha}l}{V}\right)qAl, \tag{10}$$

where l is the reference length, C_m is the restoring torque coefficient, $C_m^{\dot{\alpha}}$ is the damping torque coefficient. The aerodynamic coefficients C_D, C_L, C_m, $C_m^{\dot{\alpha}}$ are calculated using the Newton impact theory [16]. The accelerations $\ddot{\gamma}$ and $\ddot{\theta}$ in equation (9) can be obtained from equations (6) and (8), respectively, by differentiation with respect to time:
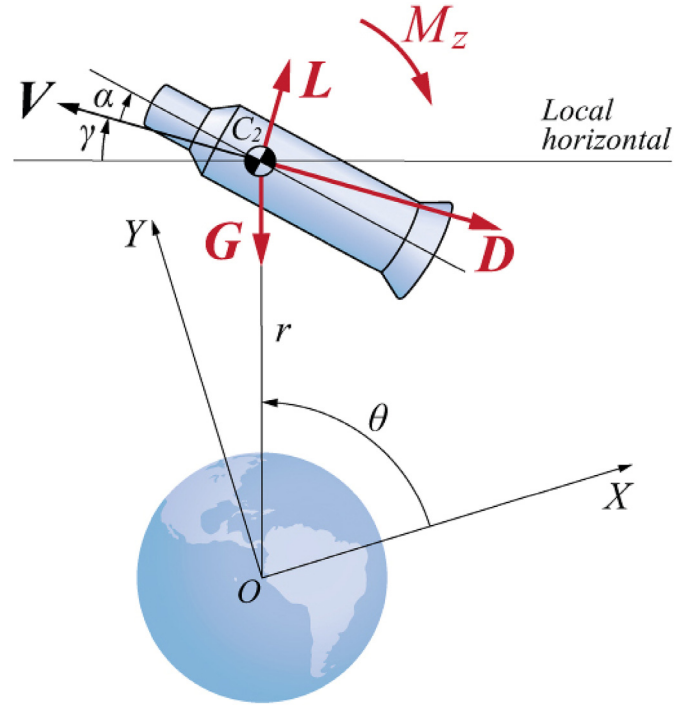
Fig. 2. Forces and torques acting on the stage during reentry.

$$\ddot{\gamma} = \frac{A}{2m_2}\left(C_L V\frac{d\rho}{dr}\dot{r} + C_L\dot{V}\rho + V\rho\frac{dC_L}{d\alpha}\dot{\alpha}\right) - \frac{V\dot{r}\cos\gamma}{r^2} + \frac{\dot{V}\cos\gamma}{r} + \frac{2g\dot{r}\cos\gamma}{rV} + \frac{Vg\cos\gamma}{V^2} - \frac{V\dot{\gamma}\sin\gamma}{r} + \frac{\dot{\gamma}g\sin\gamma}{V}, \tag{11}$$

$$\ddot{\theta} = \frac{V\dot{r}\cos\gamma}{r^2} - \frac{\dot{V}\cos\gamma}{r} + \frac{V\dot{\gamma}\sin\gamma}{r}. \tag{12}$$

The main cause of objects breakup in the atmosphere are the distributed aerodynamic loads. Their intensity can be taken to be proportional to the longitudinal n_x and transverse n_y overloads, which are defined as

$$n_x = \frac{D}{m_2 g}, \quad n_y = \frac{L}{m_2 g}. \tag{13}$$

Let as calculate thermal loads acting on the stage during its descent into the atmosphere. The heat flows are estimated for the stagnation point. The convective heat flux q_c can be calculated by the semi-empirical formula [17].

$$q_c = b\frac{\sqrt{\rho}}{\sqrt{R_s}}V^{3.15}, \tag{14}$$

where R_s is the radius of the surface at the stagnation point, $b = 5.5164\cdot10^{-5}\,kg^{1/2}s^{0.15}m^{-1.15}$ is the empirical coefficient. The total amount of heat which is transmitted to the stagnation point during the descent is defined as

$$Q = \int q_c dt. \tag{15}$$

3.4. Debris dispersion

The motion of individual debris fragments (Fig. 1) can be described by the following equations:

$$\dot{V}_i = -\frac{q_i}{\beta_i} - \frac{\mu\sin\gamma_i}{r_i^2}, \tag{16}$$

$$\dot{\gamma}_i = -\frac{\mu\cos\gamma}{V_i r_i^2} + \frac{V_i\cos\gamma_i}{r_i}, \tag{17}$$

$$\dot{r}_i = V_i \sin \gamma_i, \tag{18}$$

$$\dot{\theta}_i = \frac{V_i \cos \gamma_i}{r_i}, \tag{19}$$

where $i = 1...N$ is the number of the fragment, $\beta_i = \frac{m_i}{C_{D_i} A_i}$ is the ballistic coefficient, m_i, C_{D_i}, A_i are the mass, drag coefficient and reference area of the fragment, respectively.

We assume that the debris impact footprint on the surface of the Earth has the shape of an ellipse with semi-axes a and b. The semi-major axis can be expressed as

$$a = \frac{(\theta_{\max} - \theta_{\min})R_e}{2}, \tag{20}$$

where $R_e = 6371$ km is the mean radius of the Earth, and $\theta_{\max}$ and $\theta_{\min}$ are the maximum and minimum values of the true anomaly among all debris fragments at the moment of reaching the surface, i.e. when. $r = R_e$.

There can be two cases of stage disintegration: without an explosion and with an explosion, the latter resulting in larger footprint extent [18]. In the first case, the initial velocity of the fragment is equal to the velocity of the center of mass of the stage before breakup. In the second case, an increment ΔV_i is added to this velocity. The direction of the increment is determined by the random change of the flight path angle $\Delta \gamma_i$ [19].

4. Numerical simulation

For numerical simulation, the Ariane H10 upper stage is chosen. This rocket body consists of three main parts (Fig. 3). The first part is the engine. The central part is the H10 stage which has two propellant tanks. It consists of a cylinder with two hemispherical bulkheads. The third part is the vehicle equipment bay (VEB) with adaptor.

All of the upper stage parameters given in Table 1 were provided by the Center National d'Etudes Spatiales (CNES) [20]. To calculate the aerodynamic coefficients of the stage, we also need to know the position of the center of mass. It is determined by the distance x_C between this point and the nozzle edge. For the Ariane 4 H10 stage, it appears to be equal to 4 m. This value was obtained as follows. Within the

Fig. 3. Ariane H10 upper stage [20] and its 3D model.

Table 1
Ariane H10 upper stage parameters [20].

Parameter	Value
Total mass	2154 kg
Length	11.183 m
Maximal principal moment of inertia	28000 kg m^2
Central part mass	700 kg
Central part diameter	2.6 m
Central part length	7.372 m
Propellant tanks material	7020 alloy
Propellant tanks material density	2780 kg m^{-3}

assumption that the engine and the VEB & adaptor are point masses and the tanks in the central part can be modeled by one thin-walled cylinder, the distance x_C can be found from the following equations

$$x_C = \frac{m_e x_e + m_t x_t + m_{VEB} x_{VEB}}{m_2}, \tag{21}$$

$$m_2 = m_e + m_t + m_{VEB}, \tag{22}$$

$$J_z = m_e(x_C - x_e)^2 + \left(J_{z_t} + m_t(x_C - x_t)^2\right) + m_{VEB}(x_C - x_{VEB})^2, \tag{23}$$

$$m_t = \rho_t(\pi R^2 L - \pi(R-\delta)^2(L-2\delta)), \tag{24}$$

$$J_{z_t} = \frac{\delta \pi \rho_t R}{6}(L^3 + 3L^2R + 6LR^2 + 3R^3), \tag{25}$$

where m_e is the mass of the engine, m_{VEB} is the mass of the VEB & adaptor, m_t, R, L, δ are the mass, radius, length and wall thickness of the tank, respectively, ρ_t is the density of the tank material, J_{z_t} is the maximal principal moment of inertia of the tank, x_e, x_t, x_{VEB} are the distances between the nozzle edge and the centers of mass of the engine, tank and VEB & adaptor, respectively. These distances were estimated from Fig. 3 assuming that the centers of mass of the parts coincide with their geometric centers.

The aerodynamic coefficients of the stage were calculated using Newton impact theory. Their dependence on the angle of attack can be represented by Fourier series

$$f(\alpha) = \frac{a_0}{2} + \sum_{k=1}^{4}(a_k \cos k\alpha + b_k \sin k\alpha), \tag{26}$$

where $f = (C_D \quad C_L \quad C_m \quad C_m^\alpha)$. The coefficients a_0, a_k and b_k for the Ariane H10 stage are given in Table 2.

It can be seen from Table 2 that the functions $C_D(\alpha)$ and $C_m^\alpha(\alpha)$ are even, while $C_L(\alpha)$ and $C_m(\alpha)$ are odd. All the functions are shown in Fig. 4 by solid lines.

First of all, we focus on the towing phase of the ADR process. Towing is performed by the tug, which mass and thrust are similar to a rocket upper stage [4]. We take the most fuel-efficient case, when the maneuver is performed near the apoapsis, at the altitude h_a (Fig. 1). So for the towing phase we have

$m_1 = 2500$ kg, $F = 2000$ N, $h_a = 684$ km, $\theta_0 = \pi$, $e_0 = 0.001$.

As the result of the towing, the orbital velocity of the stage decreases by a certain amount ΔV. Higher values of ΔV correspond to lower altitudes of the stage periapsis h_p at the end of the towing and to lower times to reach the edge of the atmosphere T_{100km} during reentry (Fig. 5). The values of the orbital parameters at the end of the towing phase allow to calculate the initial conditions of the motion of the center of mass of the stage during the second phase. We assume that the initial angle of attack of the stage is equal to zero, while the initial angular velocity may vary from 0.075 to 0.2 radians per second.

Fig. 5 shows that, if an urgent removal of the stage is not required, it is not necessary to slow down the speed of the stage significantly: it is sufficient to lower its periapsis to h_p=200–300 km (Fig. 1). This is less fuel-demanding, but at the same time can induce the stage reentry within 1–3 months, which is acceptable.

Fig. 6 illustrates the evolution the kinematic parameters of the stage
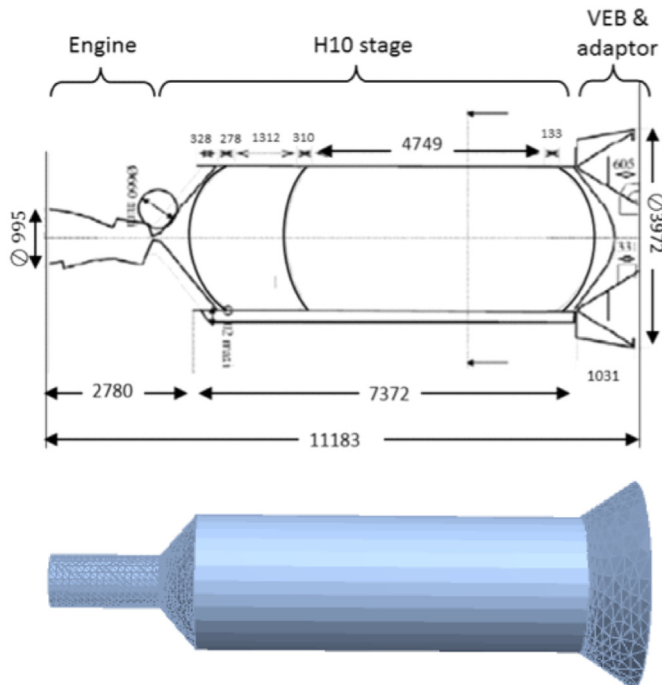
Table 2
Coefficients of the Fourier series of the functions $C_D(\alpha)$, $C_L(\alpha)$, $C_m(\alpha)$, $C_m^{\dot{\alpha}}(\alpha)$.

	a_0	a_1	a_2	a_3	a_4	b_1	b_2	b_3	b_4
C_D	8.4879	−0.4333	−1.3651	−0.8058	0.4688	0	0	0	0
C_L	0	0	0	0	0	0.1444	0.9101	0.8058	−0.6251
C_m	0	0	0	0	0	−1.2073	−0.3201	0.1072	0
$C_m^{\dot{\alpha}}$	−2.1072	−0.4197	0.4310	0.0003	0.0280	0	0	0	0
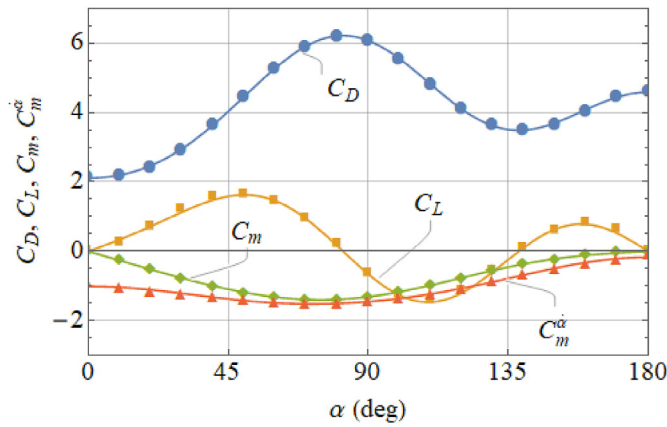
Fig. 4. Aerodynamic coefficients of the Ariane H10 upper stage (dots: Newton impact theory, solid lines: Fourier series representation).
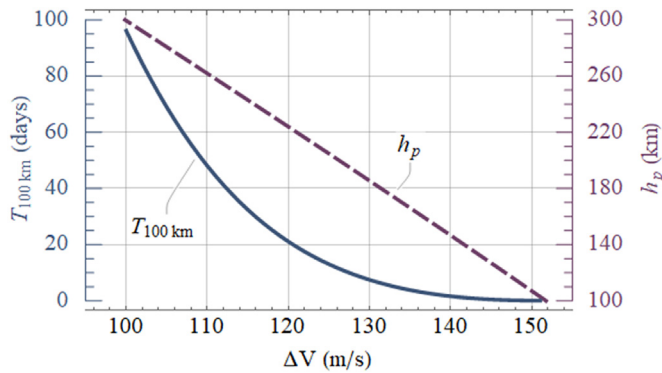
Fig. 5. Periapsis altitude at the end of the towing and time to reach the edge of the atmosphere (residual angular velocity 0.15 rad/s).
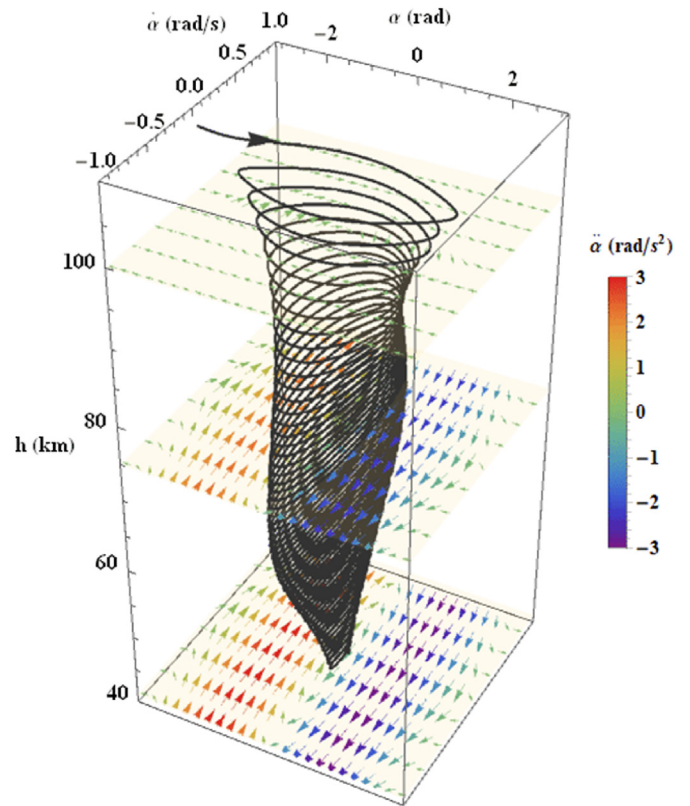
Fig. 7. Three-dimensional phase diagram of the oscillation of the stage during the descent. (residual angular velocity 0.15 rad/s, periapsis altitude after towing 125 km).

during the second phase, after the transition of the rotation into oscillation. The presence of the maximum on the dynamic pressure curve is typical. This is due to the fact that during the descent the velocity of the stage decreases while the air density increases. The evolution of the
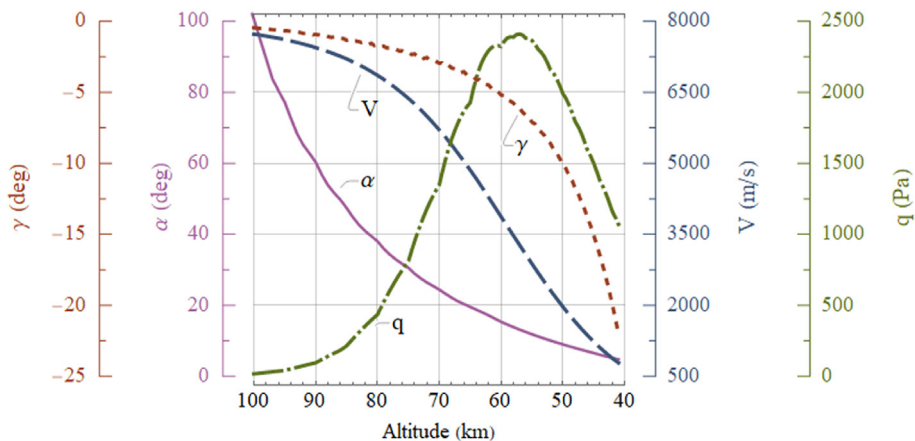
Fig. 6. Evolution of the kinematic parameters of the stage during the descent (residual angular velocity 0.15 rad/s, periapsis altitude after towing 125 km).
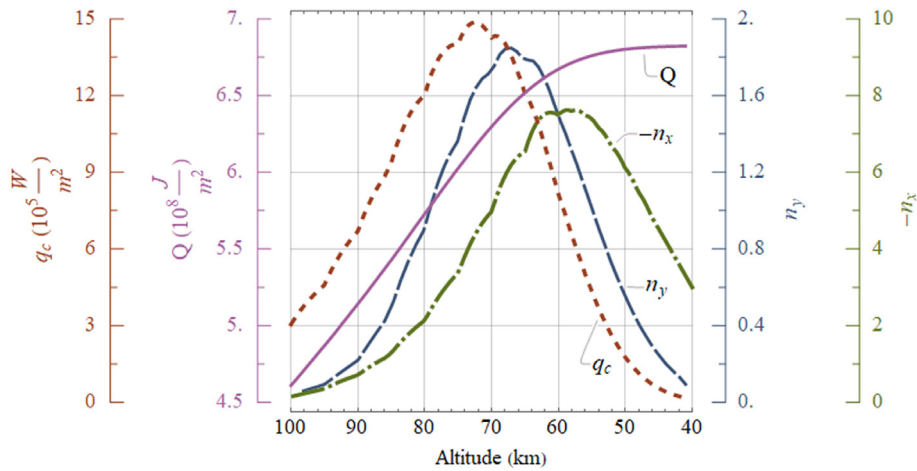
Fig. 8. Evolution of the factors causing the breakup (residual angular velocity 0.15 rad/s, periapsis altitude after towing 125 km, radius of the surface at the stagnation point 5 cm).

attitude motion of the stage during reentry can be illustrated by a three-dimensional phase diagram (Fig. 7). It shows that the absolute values of the angular velocity change in a similar way than the dynamic pressure, while the amplitude of the angle of attack decreases during all the descent due to the damping torque.

Fig. 8 depicts the evolution of the factors that directly cause the breakup of the stage during the descent: transverse n_y and longitudinal n_x overloads, as well as the heat flux q_c and total heat Q. It can be seen that, if the breakup does not occur, the stage will successively pass the peaks of the q_c, n_y, and n_x curves. The total heat Q increases during almost all the descent and becomes constant when the stage reaches the altitude of about 50 km. As we assume that for a slender vehicle the most important factor is the transverse overload n_y, let us examine the dependence of its peak magnitudes on the angular velocity of the stage $\dot\alpha_0$ after separation from the tug (Fig. 9). In the specified range of initial angular velocities, the transverse overload increases with increasing $\dot\alpha_0$. For any slender vehicle there exists a maximum transverse overload n_y^{max}, reaching which it will break up. If this value is known, it is possible to predict the breakup altitude. For the rocket body under consideration we assume $n_y^{max} = 1$ (horizontal dashed line in Fig. 9). The intersections of this line with the transverse overload curves give the minimum breakup altitudes for different values of $\dot\alpha_0$.

The dependence of the breakup altitude on the initial angular velocity of the stage is shown in Fig. 10. It is noticeable that the stage under discussion appears to have its maximum breakup altitude at about 80 km.

Fig. 10 also represents the dependence of the stabilization altitude on the initial angular velocity of the stage. Unlike the breakup altitude, this parameter decreases with increasing initial angular velocity of the stage. Notice that there exists an altitude at which the oscillation is guaranteed to begin, even when $\dot\alpha_0$ is high. For the discussed stage, it is
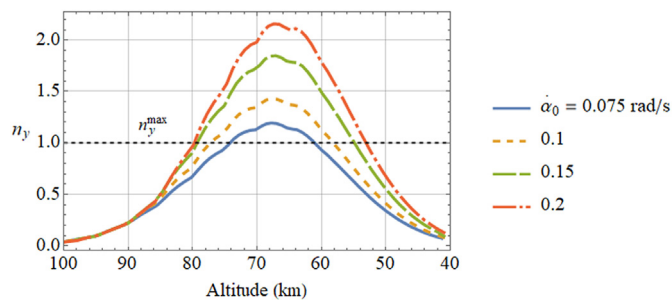
Fig. 10. Dependences of the stabilization and breakup altitudes on the residual angular velocity (periapsis altitude after towing 125 km).

about 104 km.

To estimate the size of the debris impact footprint, we simulate the motion of the fragments for two cases: when the stage is disintegrating without an explosion and when it is disintegrating with an explosion. In each numerical simulation the number of fragments N is 100. The values of the ballistic coefficient β_i are taken from the uniform distribution between 3.75 and 6.25 kg/m². In case of explosion, the increments $\Delta V_i = 100$ m/s and $\Delta\gamma_i$ are added to the velocity and flight path angle of each fragment, respectively. The increments of the flight path angle are taken from the uniform distribution on $[0, 2\pi]$. The dependence of the major axis $2a$ of the ellipse representing the footprint on the initial angular velocity of the stage is shown in Fig. 11.

In order to draw the ellipse on the surface of the Earth, one has to set the ratio between its semi-axes b and a. For a better representation of the results, we can also draw the impact points on the Earth's surface, each point having two coordinates. One of them is the distance x_i between the point and the center of the ellipse, measured along the major axis. This coordinate is obtained from the numerical simulation of the motion of the fragments. The second coordinate y_i, measured along the minor axis, is taken from the uniform distribution on $\left[-\frac{b}{a}\sqrt{a^2 - x_i^2}, \frac{b}{a}\sqrt{a^2 - x_i^2}\right]$. Fig. 12 allows to estimate the size of the footprints when $\frac{b}{a} = \frac{1}{2}$.

As it was shown above, the residual angular velocity of the stage after separation from the tug determines the breakup altitude. The latter, in its turn, determines the position of the debris impact

Fig. 9. Evolution of the transverse overload peak magnitudes during the descent (periapsis altitude after towing 125 km).
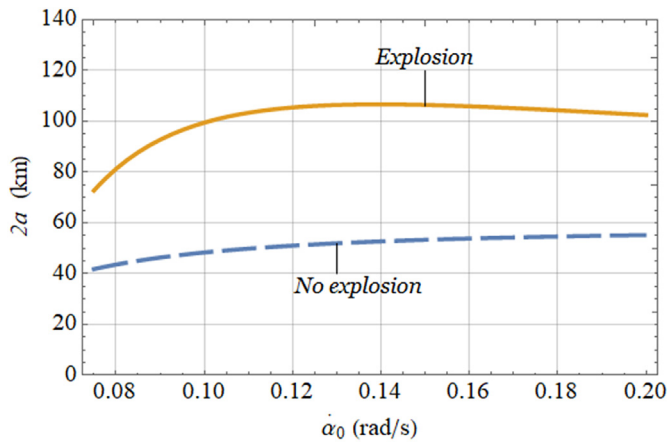
Fig. 11. Dependence of the footprint major axis on the residual angular velocity of the stage (periapsis altitude after towing 125 km).
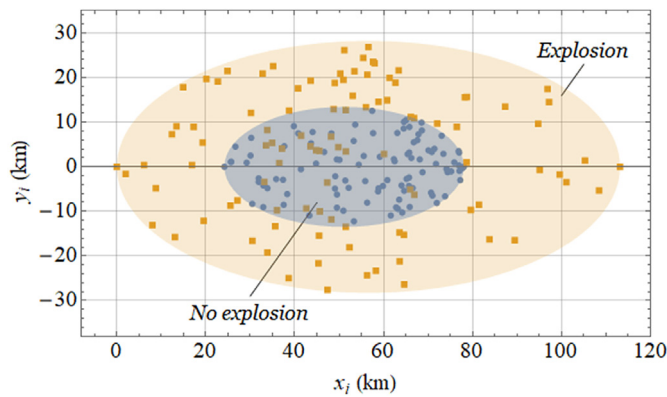
Fig. 12. Debris impact footprints (periapsis altitude after towing 125 km, residual angular velocity 0.15 rad/s).

footprint on the surface of the Earth: the higher the breakup altitude, the further along the path the debris fragments fall (Fig. 13).

The numerical simulation has shown that the extent of the debris impact footprint significantly depends on the attitude motion of the stage. This is explained by the fact that the attitude motion influences the lift and drag coefficients of the stage and therefore the overloads that cause its breakup.

5. Conclusion

In this paper, a spent upper stage removal scenario has been discussed. It includes three phases: a relatively short phase of tether-assisted deorbiting; the unconstrained motion of the stage in the low-density atmosphere until the stage breaks up; the motion of the debris fragments after the breakup. In the first phase, the Gauss planetary equations were used to determine the perigee altitude of the transfer orbit and, consequently, the initial conditions for the subsequent motion of the center of mass of the stage. In the second phase, the descent of the stage into the low-density atmosphere was examined taking into account the attitude motion. At a certain altitude the stage breaks up, reaching the critical value of the transversal overload caused by the aerodynamic forces. The Newton impact theory was used to determine the coefficients of the aerodynamic forces and torques for given geometrical characteristics of the stage. Since the aerodynamic coefficients are periodic functions of the angle of attack, they were represented as trigonometric Fourier series to simplify the calculations. In the third phase, to estimate the size of the debris impact footprint on the surface of the Earth, the motion of individual fragments, modeled as point masses, was studied.

The results of the numerical simulation of removal of an upper stage of the Ariane 4 rocket show that reducing the residual angular velocity of the stage at the moment of separation from the tug from 0.2 to 0.075 rad/s will decrease the breakup altitude from 80 to 72 km (by 10%), which will cause the reduction of the size of the debris impact footprint by 30%, on average. An even larger decrease (approximately by 50%) can be expected if the breakup without explosion is ensured.

This study has shown that the breakup altitude of the stage, which determines the size of the debris impact footprint, significantly depends on the attitude motion of the stage in the low-density atmosphere after separation from the tug. Decreasing of the residual angular velocity of the stage at the moment of separation reduces the breakup altitude and, consequently, the extent of the debris impact footprint. The breakup accompanied by an explosion obviously leads to a larger footprint. Therefore, to reduce its size, it is necessary to passivate the stage before the separation from the tug. The results of this study can be used for the future spent upper stages removal missions planning.

Declaration of competing interest

The authors declare that they have no conflict of interest.
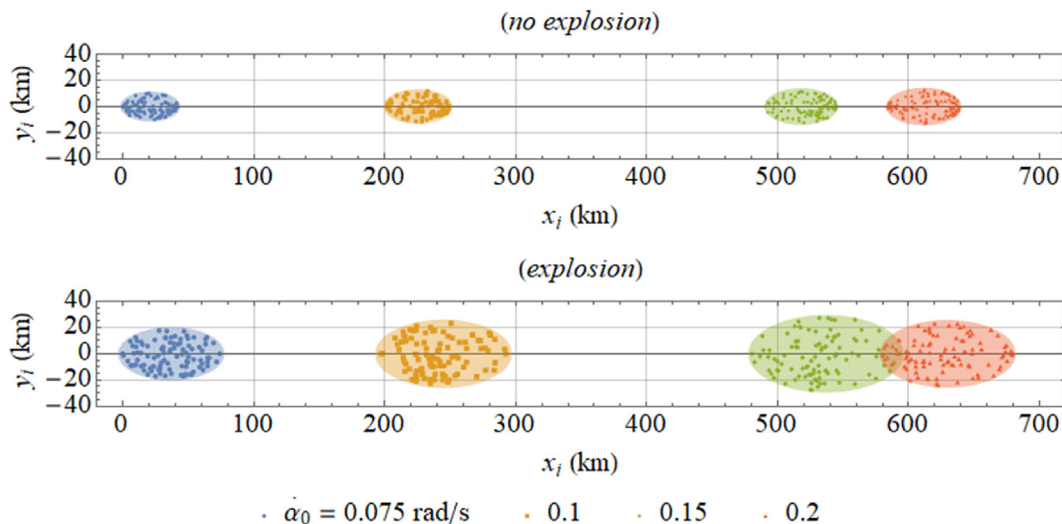
Fig. 13. Debris impact footprints (periapsis altitude after towing 125 km).

Acknowledgements

References

[1] C.P. Mark, S. Kamath, Review of active space debris removal methods, Space Policy 47 (2019) 194–206, https://doi.org/10.1016/j.spacepol.2018.12.005.

[2] C. Pardini, L. Anselmo, Characterization of abandoned rocket body families for active removal, Acta Astronaut. 126 (2016) 243–257, https://doi.org/10.1016/j.actaastro.2016.04.035.

[3] K. Kumar, M. Jankovic, N. Ortiz Gómez, J.M.R. Martin, F. Topputo, S.J.I. Walker, F. Kirchner, M. Vasile, Agora: mission to demonstrate technologies to actively remove Ariane rocket bodies, Proc. 66th Int. Astronaut. Congr. 2015, pp. 1–16 https://iafastro.directory/iac/archive/browse/IAC-15/A6/6/28851/.

[4] L. Jasper, H. Schaub, Input shaped large thrust maneuver with a tethered debris object, Acta Astronaut. 96 (2014) 128–137, https://doi.org/10.1016/j.actaastro.2013.11.005.

[5] B.W. Barbee, S. Alfano, E. Piñon, K. Gold, D. Gaylor, Design of spacecraft missions to remove multiple orbital debris objects, Adv. Astronaut. Sci. 144 (2012) 93–110.

[6] M. Kanazaki, Y. Yamada, M. Nakamiya, Trajectory optimization of a satellite for multiple active space debris removal based on a method for the traveling serviceman problem, Proc. - 2017 21st Asia Pacific, Symp. Intell. Evol. Syst. IES 2017. 2017-Janua, 2017, pp. 31–66, , https://doi.org/10.1109/IESYS.2017.8233562.

[7] J.L. Forshaw, G.S. Aglietti, T. Salmon, I. Retat, M. Roe, C. Burgess, T. Chabot, A. Pisseloup, A. Phipps, C. Bernal, F. Chaumette, A. Pollini, W.H. Steyn, Final payload test results for the remove debris active debris removal mission, Acta Astronaut. 138 (2017) 326–342, https://doi.org/10.1016/j.actaastro.2017.06.003.

[8] E.M. Botta, I. Sharf, A.K. Misra, Contact dynamics modeling and simulation of tether nets for space-debris capture, J. Guid. Control Dyn. 40 (2016) 110–123, https://doi.org/10.2514/1.g000677.

[9] N. Bérend, X. Olive, Bi-objective optimization of a multiple-target active debris removal mission, Acta Astronaut. 122 (2016) 324–335, https://doi.org/10.1016/j.actaastro.2016.02.005.

[10] M. Cerf, Multiple space debris collecting mission—debris selection and trajectory optimization, J. Optim. Theory Appl. 156 (2013) 761–796.

[11] C. Bombardelli, J. Pelaez, Ion Beam Shepherd for Contactless Space Debris Removal, (2011), pp. 1–9 http://arxiv.org/abs/1102.1289.

[12] Z. Wu, R. Hu, X. Qu, X. Wang, Z. Wu, Space debris reentry analysis methods and tools, Chin. J. Aeronaut. 24 (2011) 387–395, https://doi.org/10.1016/S1000-9361(11)60046-0.

[13] U S S Atmosphere, National Oceanic and Atmospheric Administration, Natl. Aeronaut. Sp. Adm. United States Air Force, Washington, DC, 1976.

[14] H.D. Curtis, Orbital Mechanics for Engineering Students, Butterworth-Heinemann, 2013.

[15] V.S. Aslanov, Rigid Body Dynamics for Space Applications, Butterworth-Heinemann Press, Oxford, 2017.

[16] P. Gallais, Atmospheric Re-entry Vehicle Mechanics, Springer Science & Business Media, 2007.

[17] C. Weiland, Computational Space Flight Mechanics, Springer Science & Business Media, 2010.

[18] A. Martinez Torio, D. Delorme, L. Rozenberg, V. Guenard, F. Bignalet-Cazalet, Design-to-safety: analysis of the explosion and fragmentation influence on inert debris impact footprints and mitigation solutions for innovative launcher concepts, J. Sp. Saf. Eng. 5 (2018) 184–191, https://doi.org/10.1016/j.jsse.2018.09.001.

[19] M. Reyhanoglu, J. Alvarado, Estimation of debris dispersion due to a space vehicle breakup during reentry, Acta Astronaut. 86 (2013) 211–218, https://doi.org/10.1016/j.actaastro.2013.01.018.

[20] N. Ortiz Gómez, S.J.I. Walker, Eddy currents applied to de-tumbling of space debris: analysis and validation of approximate proposed methods, Acta Astronaut. 114 (2015) 34–53, https://doi.org/10.1016/j.actaastro.2015.04.012.